2021

Flow Boiling Heat Transfer And Pressure Drop Characteristics Of R1234yf In A Dimpled Flat Duct

Yuping Gao
Creative Thermal Solutions Inc, USA

Ye Feng
Creative Thermal Solutions Inc, USA

Ke Tang
Creative Thermal Solutions Inc, USA, ke.tang@creativethermalsolutions.com

Pega Hrnjak
Creative Thermal Solutions Inc, USA

Flow Boiling Heat Transfer and Pressure Drop Characteristics of R1234yf in a Dimpled Flat Duct

Yuping GAO[1], Ye FENG[1], Ke TANG[1,2,*], Pega HRNJAK[1,2]

[1]Creative Thermal Solutions, Inc.,
Urbana, Illinois, USA
yuping.gao@creativethermalsolutions.com

[2] University of Illinois at Urbana-Champaign, Mechanical Science and Engineering,
Urbana, Illinois, USA
ketang@illinois.edu

* Corresponding Author

ABSTRACT

Among various heat transfer enhancement technologies, the dimpled surface, which is inspired by the resistance reduction characteristics of the specific concaves on golf balls, has the potential to improve heat transfer with a relatively low pressure-drop penalty. More and more applications of dimpled surfaces in heat exchangers have shown up in industries. However, the lack of experimental data, especially the heat transfer and pressure drop data for liquid-and-vapor two-phase flow, inside the dimpled flow channels prevents the good design of the dimpled heat exchangers. In this study, a facility has been designed and built to investigate the heat transfer and pressure drop of flow-boiling R1234yf in a dimpled flat duct. The details of the facility, especially the test section, are presented. A microscope is used to measure the geometrical dimensions of the dimpled flat tube. The heat loss is tested and the heat balance is checked before the experiments. The experiments are performed at mass flux from 100 to 200 kg m^{-2} s^{-1}, heat flux of 5 kW m^{-2}, saturation temperature of 15 ^{o}C, and vapor quality from 0.1 to 0.95. The experimental results are presented and discussed in detail.

1. INTRODUCTION

According to whether the external power input is required, the enhanced heat transfer technology can be roughly divided into two categories: active technology and passive technology (Bergles, 2001). Compared with active technology, passive technology can realize heat transfer enhancement by using rough surfaces with fins, groove threads, and dimples. Therefore, passive technology is used more often and extensively for its simple operation, low cost, and efficient enhancement due to no additional external power input needed. Among these modified surfaces, the dimpled surface, which is inspired by the resistance reduction characteristics of the specific concaves on golf balls, has the potential to improve heat transfer with a relatively low pressure-drop penalty (Bearman and Harvey, 1976). More and more applications of dimpled surfaces in heat exchangers have shown up in industries (Rashidi *et al*., 2019). However, the lack of experimental data, especially the heat transfer and pressure drop data for liquid-and-vapor two-phase flow, inside the dimpled flow channels prevents the good design of the dimpled heat exchangers.

In our previous studies (Tang *et al*., 2020; Gao *et al*.,2020), the flow-boiling heat transfer and pressure drop characteristics of R134a and its alternative R1234ze(E) inside a dimpled flat duct are investigated. Another promising alternative for R134a is R1234yf, which has been used in many air-conditioning and refrigeration applications. However, R1234yf has different thermophysical properties from R134a and R1234ze(E). In this study, the flow-boiling heat transfer and pressure drop characteristics of R1234yf in the dimpled flat duct are investigated.

2. EXPERIMENTAL SETUP

2.1 Test Facility

The test facility has been firstly introduced in Tang *et al*. (2020) to study flow boiling heat transfer and pressure drop of R134a in a dimpled flat duct. The facility can measure flow boiling heat transfer coefficient and two-phase pressure drop under given mass flux, heat flux, saturation temperature, and vapor quality. The test facility is composed of three loops: refrigerant loop, water loop, and glycol loop, as shown in Figure 1.

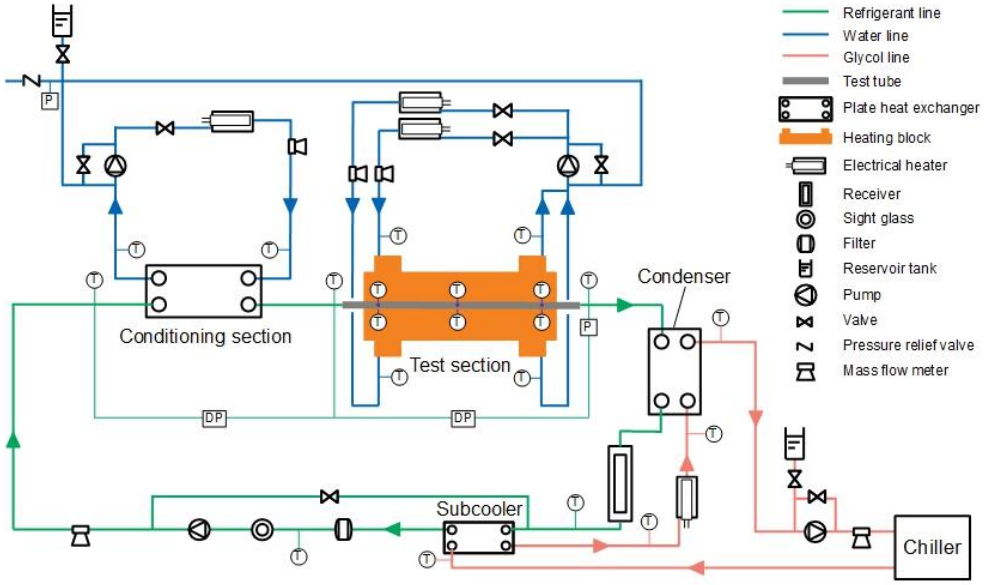

Figure 1: Schematic diagram of test facility (Tang *et al*. 2020)

The liquid refrigerant from the gear pump first goes into a mass flow meter. The mass flow rate of refrigerant is controlled by the VFD (Variable Frequency Drive) of the pump. The conditioning section is a plate heat exchanger, in which the liquid refrigerant is heated to a certain vapor quality by the flowing water. The vapor quality is determined by the water flow rate and temperature in the water loop of the conditioning section. The two-phase refrigerant then comes into the test section to measure the heat transfer coefficient and pressure drop. The heat flux in the test section is adjusted by the water flow rate and temperature in the water loop. The pressure in the test section is regulated by changing the condensation rate in the condenser, which is controlled by the flow rate and temperature of the glycol. The condensed refrigerant returns to the receiver beneath the condenser. A subcooler is used to subcool the liquid refrigerant before it enters the pump.

Table 1: Information about instrumentations used

Instrument	Model	Range	Accuracy
Thermocouple	T-type	-200 to 350 °C	±0.1 °C
Barometer sensor (P_{atm})	BMP280	30 to 110 kPa	±0.1 kPa
Gauge pressure sensor ($P_{out,ts,gauge}$)	Rosemount 3051CG5A	0 to 600 kPa	±0.065% FS
Differential pressure sensor (ΔP_{cs})	Rosemount 3051CD2A	0 to 60 kPa	±0.04% FS
Differential pressure sensor (ΔP_{ts})	Rosemount 3051CD1A	0 to 6 kPa	±0.1% FS
Differential pressure sensor (ΔP_{ts})	Rosemount 3051CD2A	0 to 60 kPa	±0.04% FS
Mass flow meter ($\dot{m}_{ref}$)	Micro Motion CFM010	0 to 15 g s^{-1}	±0.1%
Mass flow meter ($\dot{m}_{wat,cs}$)	Micro Motion CFM025	0 to 100 g s^{-1}	±0.1%
Mass flow meter ($\dot{m}_{wat,ts,top}$)	Micro Motion CFM010	0 to 5 g s^{-1}	±0.1%
Mass flow meter ($\dot{m}_{wat,ts,bot}$)	Micro Motion CFM010	0 to 5 g s^{-1}	±0.1%

The temperatures in the experiments are measured by T-type thermocouple probes, including refrigerant temperatures, water temperatures, glycol temperatures, and the wall temperatures in the test section. All the thermocouples have been calibrated before the experiments. For the pressure measurements, a barometer pressure sensor is used to measure the atmospheric pressure. A gauge pressure sensor is used to measure the refrigerant pressure at the outlet of the test section. A differential pressure sensor is used to measure the pressure drop of refrigerant across the conditioning section, and two differential pressure sensors with different ranges are used to measure the pressure drop of refrigerant across the test section. The mass flow rates of refrigerant and water are measured by Coriolis mass flow meters. The information about all instrumentations used is tabulated in Table 1.

2.2 Test Section

The schematic and picture of the test section are shown in Figure 2. The dimples are arranged in a staggered manner on both sides of the flat duct. The two ends of the dimpled flat duct are brazed with two flanges as the connectors. The test section is sandwiched by two heating blocks, which are made of aluminum alloy with high thermal conductivity. 12 thermocouples are soldered on the top and bottom walls of the dimpled flat duct to measure the wall temperature.

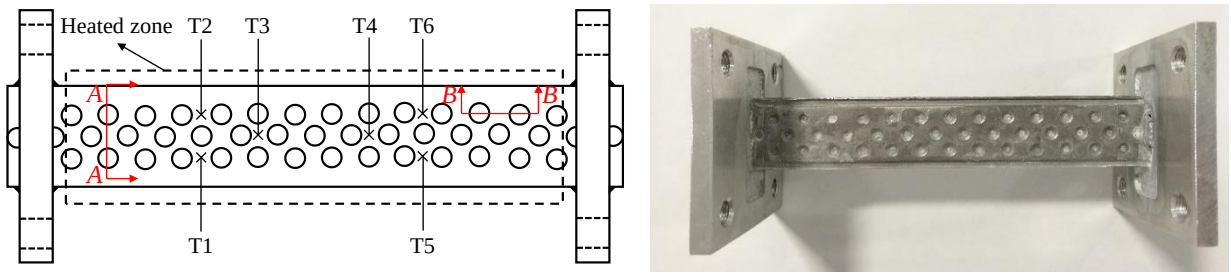

Figure 2: Schematic (a) and picture (b) of test section

A microscope is used to measure the geometrical dimensions of the dimpled flat tube. The A-A and B-B cross-sections in Figure 2(a) have been captured using two additional pieces of the dimpled flat duct, as shown in Figure 3. The measured geometrical dimensions of the dimpled flat duct are summarized in Table 2. The cross-sectional area A_c and heat transfer area A_{ht} of the dimpled flat duct are determined as 3.532×10^{-5} m^2 and 5.625×10^{-3} m^2 according to the method in our previous study (Tang *et al*. 2020).

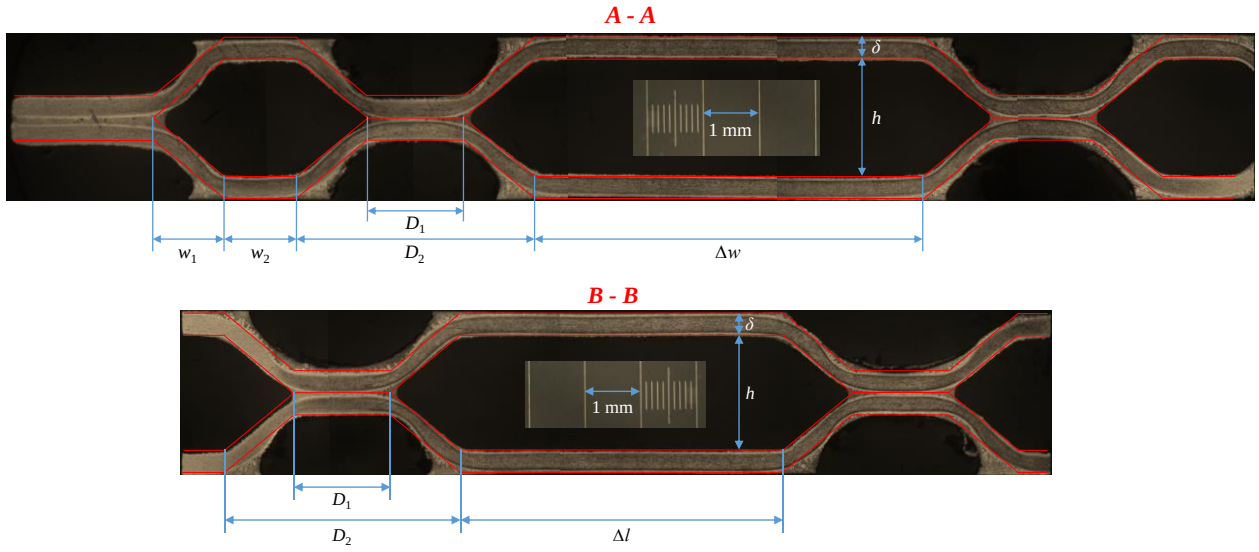

Figure 3: Cross-sections of dimpled flat duct

Table 2: Geometrical dimensions of test section

Symbol	Parameter	Dimension [m]
L_{dim}	Length of dimpled flat duct	1.537×10^{-1}
$L_{dim,h}$	Heated length of dimpled flat duct	1.3×10^{-1}
w_1	Width of side corner	1.28×10^{-3}
w_2	Width between side corner and dimple	1.28×10^{-3}
D_1	Top diameter of dimple	1.728×10^{-3}
D_2	Bottom diameter of dimple	4.241×10^{-3}
Δw	Spanwise interval of dimple	6.964×10^{-3}
Δl	Streamwise interval of dimple	5.793×10^{-3}
h	Height of dimpled flat duct	2.069×10^{-3}
δ	Wall thickness of dimpled flat duct	4.14×10^{-4}

2.3 Heat Loss and Heat Balance

The heat loss of the test section is determined using a method where the dimpled flat duct is vacuumed while keeping water flowing in the heating blocks. In this way, the heat transfer is restricted between water and the ambient. The dependence of the heat loss with the temperature difference between water and ambient is presented in Figure 4. Furthermore, the heat balance of the test section is checked through a series of single-phase tests. Accounting for the heat loss to ambient, the relative deviations of the heat released by water and the heat absorbed by the refrigerant in the test section are within ±5%, as shown in Figure 5.

3. DATA REDUCTION

The mass flux of refrigerant in the test section G is determined as:

$$G = \frac{\dot{m}_{\mathrm{ref}}}{A_c}. \tag{1}$$

The saturation temperatures of refrigerant at the inlet of the test section $T_{sat,in,ts}$ and at the outlet of the test section $T_{sat,out,ts}$ can be determined by the corresponding pressures $P_{in,ts}$ and $P_{out,ts}$. The averaged saturation temperature in the test section T_{sat} is calculated as:

$$T_{\mathrm{sat}} = \frac{T_{\mathrm{sat,in,ts}} + T_{\mathrm{sat,out,ts}}}{2}. \tag{2}$$

The refrigerant at the inlet of the conditioning section is subcooled, thus its specific enthalpy $h_{in,cs}$ can be determined by the measured temperature $T_{in,cs}$ and pressure $P_{in,cs}$. The specific enthalpy of refrigerant at the inlet of the test section $h_{in,ts}$ is calculated as:

$$h_{\mathrm{in,ts}} = h_{\mathrm{in,cs}} + \frac{Q_{\mathrm{cs}}}{\dot{m}_{\mathrm{ref}}}, \tag{3}$$

where Q_{cs} is the heat absorbed by the refrigerant in the conditioning section. The vapor quality of refrigerant at the inlet of the test section $x_{in,ts}$ can be calculated as:

$$x_{\mathrm{in,ts}} = \frac{h_{\mathrm{in,ts}} - h_{\mathrm{l,in,ts}}}{h_{\mathrm{v,in,ts}} - h_{\mathrm{l,in,ts}}}, \tag{4}$$

where $h_{l,in,ts}$ and $h_{v,in,ts}$ are the specific enthalpies of refrigerant for saturated liquid and saturated vapor. The specific enthalpy of refrigerant at the outlet of the test section $h_{out,ts}$ is calculated as:

$$h_{\mathrm{out,ts}} = h_{\mathrm{in,ts}} + \frac{Q_{\mathrm{ts}}}{\dot{m}_{\mathrm{ref}}}, \tag{5}$$

where Q_{ts} is the heat absorbed by the refrigerant in the test section. The vapor quality of refrigerant at the outlet of the test section $x_{out,ts}$ is calculated as:

$$x_{\mathrm{out,ts}} = \frac{h_{\mathrm{out,ts}} - h_{\mathrm{l,out,ts}}}{h_{\mathrm{v,out,ts}} - h_{\mathrm{l,out,ts}}}, \tag{6}$$

where $h_{l,out,ts}$ and $h_{v,out,ts}$ are the specific enthalpies of refrigerant for saturated liquid and saturated vapor. The averaged vapor quality in the test section x is determined as:

$$x = \frac{x_{\mathrm{in,ts}} + x_{\mathrm{out,ts}}}{2}. \tag{7}$$

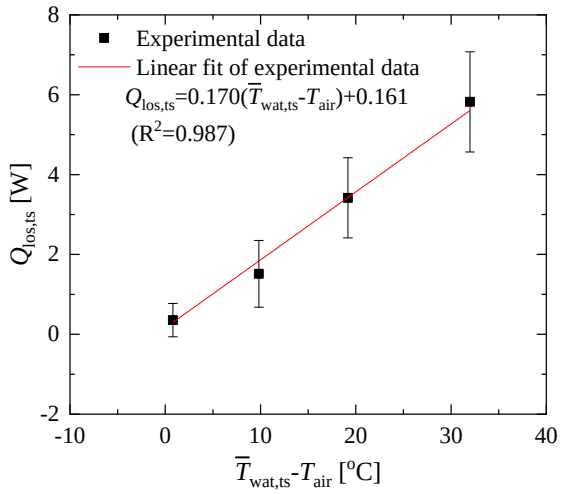

Figure 4: Heat loss of test section

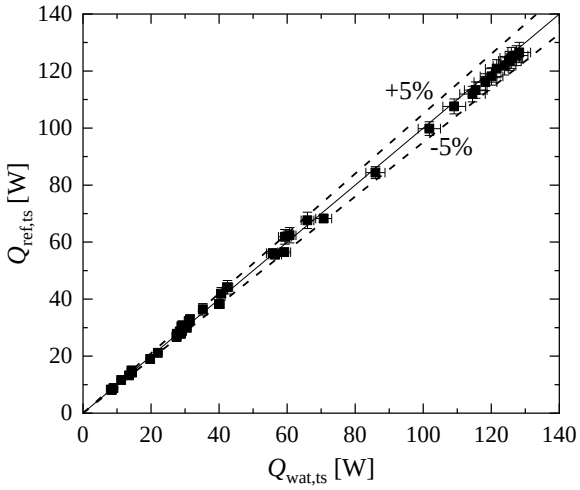

Figure 5: Heat balance of test section

The heat flux applied to the test section q is calculated as:

$$q = \frac{Q_{ts}}{A_{ht}}. \tag{8}$$

The heat transfer coefficient (HTC) of the dimpled flat duct is determined as:

$$\mathrm{HTC} = \frac{q}{T_{wal,in} - T_{sat,ts}}, \tag{9}$$

where $T_{wal,in}$ is the inner wall temperature of the heated dimpled flat duct, which is calculated by using the one-dimensional heat conduction model based on the measured temperature of the duct wall outer surface.

The measured pressure drop across the test section ΔP_{ts} is the summation of the frictional pressure drop ΔP_{fri} and the acceleration pressure drop ΔP_{acc}, therefore the frictional pressure drop ΔP_{fri} can be calculated as:

$$\Delta P_{fri} = \Delta P_{ts} - \Delta P_{acc}, \tag{10}$$

where the acceleration pressure drop ΔP_{acc} is calculated as:

$$\Delta P_{acc} = G_{ts}^2 \left\{ \left[\frac{(1-x)^2}{\rho_l (1-\alpha)} + \frac{x^2}{\rho_v \alpha} \right]_{out} - \left[\frac{(1-x)^2}{\rho_l (1-\alpha)} + \frac{x^2}{\rho_v \alpha} \right]_{in} \right\}, \tag{11}$$

where x is vapor quality, ρ_l and ρ_v are liquid density and vapor density, α is void fraction calculated by Zivi correlation (Zivi, 1964). Then, the frictional pressure gradient in the dimpled flat duct ∇P_{fri} is determined as:

$$\nabla P_{\mathrm{fri}} = \frac{\Delta P_{\mathrm{fri}}}{L_{\mathrm{dim}}}. \tag{12}$$

The standard uncertainties of the vapor quality, heat transfer coefficient, and frictional pressure gradient are determined by Engineering Equation Solver (EES) based on NIST Technical Note 1297 (Taylor and Kuyatt, 1994). The expanded uncertainties of the heat transfer coefficient and the frictional pressure gradient with 95% confidence interval are given along with the experimental data in section 4. Results and discussion.

4. RESULTS AND DISCUSSION

In this section, the experimental data of flow boiling heat transfer coefficient and frictional pressure gradient of R1234yf inside the dimpled flat duct are presented. The effects of vapor quality and mass flux on the heat transfer coefficient and frictional pressure gradient are analyzed.

4.1 Heat Transfer Coefficient

The dependences of the flow-boiling heat transfer coefficient of R1234yf inside the dimpled flat duct on the vapor quality under different mass fluxes are presented in Figure 6. The flow-boiling heat transfer coefficient increases with the vapor quality. This is attributed to the increasing vapor quality leading to increasing velocity and decreasing liquid film thickness of the two-phase flow inside the dimpled flat duct. The increasing velocity and the decreasing liquid film thickness benefit the convective evaporation heat transfer inside the dimpled flat duct. With a rise in mass flux, the flow-boiling heat transfer coefficient increases, owing to the enhancement of convective evaporation heat transfer. The dryout does not show up with the vapor quality up to 0.95, which is similar to the results of R134a and R1233zd(E) in our previous study (Gao *et al*.,2020). The possible reason is that the liquid refrigerant would be accumulated around the dimples by the surface tension force with the presence of the sharp corners. The nucleate boiling could still take place at these corners and the heat transfer coefficient is still high.

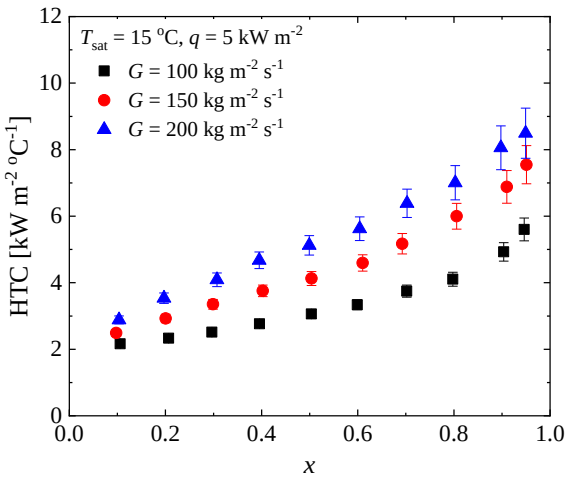

Figure 6: Dependences of flow-boiling heat transfer coefficient on vapor quality under different mass fluxes

4.2 Frictional Pressure Gradient

Figure 7 presents the dependences of the frictional pressure gradient of R1234yf inside the dimpled flat duct on the vapor quality under different mass fluxes. The frictional pressure gradient increases almost linearly with increasing vapor quality in the test range. This is attributed to the rise in the velocities of both the liquid phase and the vapor phase with increasing vapor quality. But the contribution of the vapor phase is more significant than that of the liquid phase. As for the effect of mass flux, the frictional pressure gradient increases with a rise in mass flux, owing to the increasing velocities of the liquid and vapor phases. When the mass flux is doubled from 100 kg m^{-2} s^{-1} to 200 kg m^{-2} s^{-1}, the frictional pressure gradient is increased by about 2.9 times.

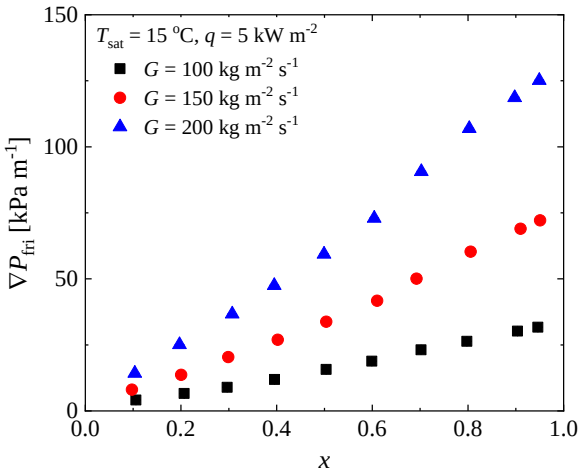

Figure 7: Dependences of flow-boiling frictional pressure gradient on vapor quality under different mass fluxes

5. CONCLUSIONS

The flow-boiling heat transfer and pressure drop of R1234yf in a dimpled flat duct are experimentally investigated. The flow-boiling heat transfer coefficient increases with vapor quality and mass flux in the test range, implying that the convective evaporation dominates the flow boiling heat transfer inside the dimpled flat duct. The dryout does not show up with the vapor quality up to 0.95, which is similar to the results of R134a and R1233zd(E) in our previous study. The possible reason is that the liquid refrigerant would be accumulated in the sharp corners around the dimples by the surface tension force, which gives the chance for the nucleate boiling to take place. The frictional pressure gradient increases almost linearly with increasing vapor quality in the test range. The effect of mass flux on the frictional pressure gradient is significant. When the mass flux is increased from 100 kg m^{-2} s^{-1} to 200 kg m^{-2} s^{-1}, the frictional pressure gradient is increased by about 2.9 times.

REFERENCE

Bearman, P. W., & Harvey, J. K. (1976). Golf ball aerodynamics. *The Aeronautical Quarterly, 27*(2), 112-122.

Bergles, A. E. (2001). The implications and challenges of enhanced heat transfer for the chemical process industries. *Chemical Engineering Research and Design*, *79*(4), 437-444.

Gao, Y., Feng, Y., Tang, K., & Hrnjak, P. (2020). Comparison of flow boiling pressure drop and heat transfer of R134a with low GWP alternative R1234ze(E) in a dimpled flat duct. *International Journal of Refrigeration*, *119*, 165-174.

Rashidi, S., Hormozi, F., Sundén, B., & Mahian, O. (2019). Energy saving in thermal energy systems using dimpled surface technology–A review on mechanisms and applications. *Applied Energy*, *250*, 1491-1547.

Tang, K., Gao, Y., Feng, Y., & Hrnjak, P. (2020). Pressure drop and heat transfer of flow boiling R134a in a dimpled flat duct. *International Journal of Heat and Mass Transfer*, *151*, 119398.

Taylor, B. N., & Kuyatt, C. E. (1994). National Institute of Standards and Technology Technical Note 1297 .

Zivi, S. M. (1964). Estimation of steady-state steam void-fraction by means of the principle of minimum entropy production.